RSC Advances

ROYAL SOCIETY OF CHEMISTRY

www.rsc.org/advances

Azo Dye Functionalized Graphene Nanoplatelets for Selective Detection of Bisphenol A and Hydrogen Peroxide†

Nael G. Yasri[a,b,c±], Ashok K. Sundramoorthy[a±], and Sundaram Gunasekaran[a,*]

[a]Department of Biological Systems Engineering

University of Wisconsin-Madison,

460 Henry Mall, Madison, WI 53706, USA

[b]Department of Chemistry

Faculty of Science, University of Aleppo, Syria

[c]Department of Chemical and Biochemical Engineering

Western University, London, Ontario, Canada.

*Corresponding author: S. Gunasekaran (guna@wisc.edu)

±Ashok K. Sundramoorthy and Nael G. Yasri have contributed equally to this work.

†Electronic supplementary information (ESI) available: A stability test of GNP-DB film modified GCE and GNP-DB film preparation on PET.

Abstract

Graphene nanoplatelets (GNP) have emerged as a promising electrode material for electrochemical sensing applications because of their high conductivity, large surface-to-volume ratio, biocompatibility, and low cost. However, GNP are not soluble in water. We dispersed GNP in water with the assistance of a tri-azo dye, Direct blue 71 (DB). Thin films prepared with GNP/DB dispersion were characterized by scanning electron microscopy (SEM), Raman spectroscopy, and UV–vis spectroscopy, which indicated the binding of DB with GNP films. The GNP/DB film coated glassy carbon electrode (GCE) exhibited high electrocatalytic activity to oxidation of bisphenol A (BPA) and reduction of hydrogen peroxide (H_2O_2). The GNP/DB film greatly enhanced the BPA oxidation peak current at +524 mV, and the H_2O_2 reduction peak current at -400 mV vs. Ag/AgCl in pH 7.0 phosphate-buffered saline (PBS) solution. The oxidation peak current was proportional to BPA concentration from 10 nM to 100 nM and 100 nM to 25 μM, with a limit of detection of 1.23 nM. The GNP/DB-modified GCE also showed remarkable decrease of over-potential for the reduction of H_2O_2 with a fast amperometric response of less than 2 s, good linear range of 10 μM to 1.9 mM, and high sensitivity of 57.6 μA/mM. The fabricated sensor shows good reproducibility and stability with limited interference. Furthermore, the sensor was successfully applied to determine BPA in spiked commercial milk and juice samples.

Keywords: Bisphenol A, graphene nanocomposite, hydrogen peroxide, electrochemical sensor, modified electrode

1. Introduction

Bisphenol A (2,2-bis(4-hydroxyphenyl)propane, BPA) is an endocrine disrupting compound[1]. BPA is widely used in plastics and epoxy resins and the widespread presence of these materials in everyday objects means that humans are being exposed to potential health risks[2], particularly following fetal or early life exposure[3]. The United States Environmental Protection Agency (US EPA) had regulated BPA intake of humans to not exceed 0.05 mg/kg of body weight per day, and the actual exposure should be far less[2]. Therefore, it is important to develop a highly sensitive and reliable method to detect the presence of even trace levels of BPA in foods and environmental samples.

Traditional analytical methods such as liquid chromatography (LC)[4], high performance liquid chromatography (HPLC)[5], and immunoassay[6] are widely used for BPA detection. However, these laboratory tests are not amenable for point-of-use monitoring. Electrochemical sensors are highly advantageous for on-site detection of variety of analytes when the electrodes are suitably fabricated and functionalized. Metal nanoparticles (NPs) and their derivatives, e.g., gold (Au)[7], cobalt (Co)[8], nickel (Ni)[9], iron (Fe(II,III))[10], zinc (Zn)[11], Mg-Al-CO_3[12], ruthenium (Ru)[13], and tungsten (W)[14], are popular candidates for electrode modification. However, when using electrodes modified with metal NPs, detection of BPA suffers from the inherent structure and oxidation susceptibility of BPA, which leads to inactivation of NPs and their derivatives due to the formation of electro-polymerized films[15].

Furthermore, inadequate treatment of BPA in aqueous environment involves, in some cases, the production of hydrogen peroxide (H_2O_2), leads to the presence of both H_2O_2 and BPA in water. H_2O_2 is an important analyte in many industries, food and clinical laboratories, and the environment[16, 17]. H_2O_2 also plays an important role in many biological and enzyme-based

reactions (e.g., the enzymatic reaction of glucose oxidase). Methods of H_2O_2 determination include traditional titration, spectrophotometry[18, 19], chemiluminescence[20] enzymatic and electrochemical biosensing[21, 22] etc. Just like BPA, trace amounts of H_2O_2 is also encountered in food samples[19]. The typical analytical methods for H_2O_2 detection suffer from interferents in real samples and they are also time-consuming as they involve many steps[21]. Recently, graphene and nitrogen-doped graphene have been used for effective electrochemical reduction of H_2O_2[23, 24]. Graphene sheets usually irreversibly agglomerates or stacks to form graphite-like structures, mainly owing to the π-π interaction and hydrophobic attraction[25]. This phenomena has generally been considered an insurmountable challenge, which prevents dispersion of graphene sheets[26] in water without the aid of a dispersing agent[27, 28]. However, stabilization of graphene sheets in water without a surfactant has been achieved via electrostatic stabilization[27] or partial oxidation on graphene sheets during electrochemical synthesis[29, 30]. At the same time, there is an ever increasing interest in chemical-doped graphene with foreign atoms as an effective method to intrinsically modify the properties of the pristine host material[31]. For example, nitrogen-doping plays a critical role in regulating the electronic properties of graphene materials[32]. The heteroatoms present in the graphitic framework, make these catalysts non-electron-neutral and consequently favors the molecular adsorption and enhances some redox reactions at the electrode interface[33]. Doped graphene is a highly efficient, metal-free, and cost-effective electrochemical catalyst for sensor applications.

Herein we report using sulfonate functionalized tri-azo dye, direct blue 71 (DB) (i.e., 1,5-naphthalenedisulfonic acid, 3-[[4-[[4-[(6-amino-1-hydroxy-3-sulfo-2-naphthyl)azo]-6- sulfo-1-naphthyl]azo]-1-naphthyl] azo]-, tetra sodium salt) to obtain an aqueous dispersion of graphene nanoplatelets (GNP) (**Scheme 1**). GNP have platelet like morphology with a diameter of ~500

nm to 25 μm and thickness of about from 5 – 25 nm. They possess high thermal, electrical, and mechanical properties. Because of low cost and easy large-scale production, GNP have received much attention in applications such as fabricating nanocomposites[34], biosensors[35], supercapacitors[26], lithium-ion batteries[36, 37] etc.

We observed that GNP could be dispersed in water with DB molecules through electrostatic repulsion. As expected, longer aromatic naphthalene based DB could effectively exfoliate GNP sheets in water and stabilize them individually even after centrifugation[38]. The dispersibility of GNP in water was enhanced with DB because the strong hydrophobic aromatic backbone of DB was stacked on graphene surface, and the sulfonic ($-SO^{3-}$) acid functional groups of DB aided in solubilizing them in water due to electrostatic repulsion[38, 39]. We formed stable thin film of GNP/DB on glassy carbon electrode (GCE) by drop-casting GNP/DB dispersion and used the GNP/DB-GCE for selective and sensitive detection of BPA and H_2O_2.

2. Experimental section

2.1 Reagents

Grade xGnP GNP was purchased from XG Sciences, Inc. DB and BPA (97% reagent) were purchased from Sigma-Aldrich. Stock solution of 10×10^{-3} M BPA was prepared in ethanol and used for further dilution. Other reagent-grade chemicals were purchased from Fisher Scientific and used as received. Stock solution of 0.1 M H_2O_2 was freshly prepared from 30% reagent (Fisher Scientific) in 125 mM PBS (pH=7) and used for further dilution. All aqueous solutions were prepared using deionized water of 18.2 MΩ.cm resistivity (EMD, Millipore).

2.2 Preparation and characterization of GNP/DB dispersion

The GNP powder (20 mg) was dispersed in 20 mL of 1 mM DB in deionized water. The solution was bath-sonicated for 10 min, followed by probe sonication (Sonics, VibraCell VCX130) for 60 min in pulse mode (5 s on, 2 s off) at 60% amplitude. The GNP/DB dispersion was centrifuged for 30 min at 4,000 rpm (Sorvall Super T21) and was quickly decanted from the tube without disturbing the precipitate. The supernatant was used to form GNP/DB film and for further characterization. All experiments were performed at room temperature (25±3 °C).

A portion of GNP/DB dispersion was vacuum filtrated (membrane pore size ~0.4 μm) and washed with deionized water until colorless filtrate was obtained. The filter paper containing the residue (GNP/DB) was dried at 60 °C. The resulting dry powder fraction (GNP/DB), pristine GNP, and DB were used for all characterization experiments.

The surface morphology of GNP and GNP/DB films were observed by scanning electron microscopy (SEM) (LEO1530, Gemini FESEM, Carl Zeiss, USA). Raman spectroscopy was performed on pristine GNP, GNP/DB, DB and on annealed GNP/DB samples using LabRAM Aramis Horiba Jobin Yvon Confocal Raman Microscope (wavelength=532 nm).

DB was removed from GNP/DB samples by heating in argon atmosphere at 500 °C for 1 h at 2 °C/min heating rate in an annealing furnace tube (NT-MDT NTEGRA). UV-vis spectra of GNP, DB and GNP/DB dispersed in DMF were obtained using a spectrophotometer (Lambda 25, PerkinElmer, USA).

2.3 Electrochemical sensor preparation

GCEs were cleaned first by polishing with alumina powder then by rinsing with deionized water, and subsequently by ultrasonicating successively for 5 min each in 0.05 M HNO_3 and ethanol solutions. Finally the GCEs were modified by drop-coating with 10 μL of GNP/DB dispersion or GNP dispersed in DMF. The modified GCEs (GNP/DB-GCE and GNP-

GCE) were left to dry at 60 °C for 1 h and washed with deionized water before use. We also prepared GNP/DB film similarly on a polyethylene terephthalate (PET) for film stability studies.

2.4 Electrochemical measurements

Electrochemical measurements, namely cyclic voltammetry (CV), electrochemical impedance spectroscopy (EIS), and differential pulse voltammetry (DPV), were performed using an electrochemical workstation (PGSTAT128N, Metrohm Autolab, B.V., The Netherlands). A 10-mL volume, three-electrode system was used with GCE, Ag/AgCl (3 M KCl), and platinum wire as working, reference, and counter electrodes, respectively. Both bare and modified GCEs were used.

EIS measurements were performed in a solution containing 2.5 mM $[Fe(CN)_6]^{4-/3-}$ and 0.1 M KCl supporting electrolyte in the frequency range of 1 to 10^6 Hz. DPV measurement of BPA was performed applying stripping steps with the following parameters: initial potential, 0.2 V; final potential, 0.6 V; amplitude, 0.05 V; pulse width, 0.2 s; pulse period, 0.5 s; scan rate = 0.01 V/s. The DPV voltammograms were recorded upon injection of BPA in the range of 10.0 nM to 25.0 µM in 125 mM PBS (pH = 7). The interferences of some organic and inorganic species such as H_2O_2, ascorbic acid, citric acid, oxalic acid, glucose, caffeine, magnesium (Mg^{2+}), calcium (Ca^{2+}), sulfate (SO_4^{2-}), iron (Fe^{2+}), copper (Cu^{2+}), zinc (Zn^{2+}), and mercury (Hg^{2+}) were investigated against 10.0 µM of BPA.

The response of GNP/DB-GCE toward H_2O_2 was measured chronoamperometrically in N_2-saturated 125 mM PBS (pH = 7) at a constant voltage (-400 mV) and the current was measured after spiking with H_2O_2.

3. Results and discussion

3.1 GNP/DB Characterization

The Raman spectra of the (i) DB, (ii) pristine GNP, (iii) GNP/DB and (iv) annealed GNP/DB film are presented in **Fig. 1a**. The Raman spectrum of GNP shows a disorder band (D) (at 1364 cm^{-1}), G peak (at 1585 cm^{-1}) and a 2D peak (at 2734 cm^{-1}) (curve ii). The G mode is a characteristic of graphene originating from the in-plane vibration of sp2 carbon atoms[40]. The presence or variation of the G mode and 2D mode can be directly used to test if the symmetry of the hexagonal graphene backbone framework has been preserved after probe sonication with DB. The Raman spectra of the GNP/DB sample exhibited a high D peak (at 1383 cm^{-1}) as well as several other new peaks besides the previously existing G and 2D peaks (**Fig. 1a**, curve iii). Generally, the D band arises from the defects involved in the double resonant Raman process and it is widely used to monitor the formation of bonds in chemically functionalized graphene[41]. The defects in the GNP/DB are caused by the formation of sp3 bonds as well as the breaking of the translational symmetry of sp2 C=C network. These are distinguished clearly from upshifting of D, G and 2D by 16, 8, 20 cm^{-1} respectively, as well as from the increases in the D peak as compared with that of the pristine GNP[42]. The upshifting of the 2D peak is due to electron doping, with charge transfer inducing the modification of the equilibrium lattice parameter[43]. The modification of the pristine backbone is also confirmed by the presence of new peaks in the GNP/DB spectrum at 1004, 1152, 1192, 1283, 1324, 1422, and 1479 cm^{-1}, which are those, attributed to the DB molecular groups grafted onto the graphene structure and was not water washable. These peaks are consistent with the original DB peaks, with almost low degree shifting. The Raman vibration bands of DB correspond to SO_3 at 1004 cm^{-1} (symmetric stretching vibration)[38, 44], C-N at 1155 cm^{-1} (symmetrical stretch), C-N at 1193 cm^{-1} (symmetric bend), CH at 1282 cm^{-1} (naphthyl bend), naphthalenic rings at 1324 cm^{-1} (symmetric vibration),

N=N at 1419 cm^{-1} N=N (stretch), N=N at 1481 cm^{-1} (valence), naphthalenic rings at 1526 cm^{-1} (stretch), C=C at 1587 cm^{-1} (stretch), and second naphthalenic rings at 1624 cm^{-1} (stretch).

Based on the Raman spectroscopy data in **Table 1,** the type of DB bonding with the graphene material is difficult to distinguish. However, it has been reported that under many reaction conditions, a combination of both covalent binding or chemisorption is accompanied with an increase in D band to G band intensity ratio (I_D/I_G); whereas, non-covalent doping or physisorption is accompanied with the G and 2D peaks shifting as well as a decrease in their intensity ratio (I_{2D}/I_G)[45] (See Table 1)[29, 45]. Thus our results provide clear evidence that DB is attached to the graphene basal plane.

In contrast, the Raman spectrum of the annealed GNP/DB sample was very different. Usually, I_D/I_G ratio serves as a convenient measure of the amount of defects in graphitic materials[44, 46], which is higher for annealed GNP/DB (0.18) than for pristine GNP (0.159) indicating that unrecoverable defects have been introduced in the GNP lattice. In addition, the 2D peak for GNP/DB has upshifted by 4 cm^{-1} compared to that of pristine GNP (**Fig. 1a**). The defects in the annealed sample was also confirmed by the presence of D′ peak (at 1634 cm^{-1})[40]. These results demonstrate that DB is indeed grafted onto the graphene structure by probe sonication, which has introduced unrecoverable changes in the graphene backbone framework.

The grafting of DB onto graphene was also observed by UV–vis spectra of GNP, DB, and GNP/DB dissolved in DMF (**Fig. 1b**). The spectrum of GNP exhibits an absorption peak at 273 nm, corresponding to the π–π* transition of aromatic C–C bonds[47]. Typically, DB exhibits absorption spectra with strong peaks in the visible (595 nm) and UV (294 nm) regions. The spectrum of the GNP/DB sample, obtained after probe sonication, exhibits a peak in the visible region (597 nm) and a shoulder in the UV region (285 nm), indicating the presence of DB on the

graphene. The peak in the UV region slightly blue-shifted, perhaps due to delocalization of the π-electron clouds based on donor/acceptor interactions between the functional groups in DB and GNP. However, the peak in the visible region is red-shifted due to the electron withdrawing effect between graphene and DB [40].

SEM images of pristine GNP and GNP/DB film are shown in **Fig. 2a and b**. The uniformity of the films formed could be easily distinguished from the two SEM images. The pristine GNP film shows randomly distributed, wrinkled or aggregated graphene sheets of various dimensions (**Fig. 2a**); whereas, GNP/DB film exhibits a fairly uniform nanocomposite structure (**Fig. 2b**). The resolution of SEM image of GNP/DB film is not as good as pristine GNP film, which is perhaps partly due to the evaporation and/or some kind of molecule vibration of DB under high energy x-ray beam.

3.2 Electrochemical characterization of the modified GCE

CV of $Fe(CN)_6]^{4-/3-}$ is an effective and convenient tool to monitor the surface modification of electrodes during each step of functionalization. The electrochemical properties of the GNP-GCE and GNP/DB-GCE were studied using 2.5 mM $Fe(CN)_6]^{4-/3-}$ and 0.1 M KCl (**Fig. 2, c and d**). The redox peak currents of $Fe(CN)_6]^{4-/3-}$ increased with GNP-GCE and GNP/DB-GCE as compared with bare GCE (**Fig. 2c**); for example, the oxidation peak current increased from 11.60 μA at bare GCE (curve i) to 13.47 μA and 16.15 μA at GNP-GCE (curve iii) and GNP/DB-GCE (curve ii), respectively (**Fig. 2c**). These results indicate that both GNP/DB and GNP films enhance the electroactive surface area of GCE. It has been reported, however, in carbon nanomaterials, chemical doping has potential to enrich free charge-carrier densities and enhance their electrical conductivity[32]. Due to higher electrocatalytic activity of the GNP/DB film, the redox current peaks at GNP/DB-GCE are higher than those at GNP-GCE.

The Nyquist plots of the bare GCE, GNP-GCE and GNP/DB-GCE are shown in **Fig. 2d.** The semicircular part in the high frequency region represents electron-transfer-limiting process with its effective diameter equal to Faradaic charge transfer resistance (R_{ct}), which is responsible for electron transfer kinetics of redox reactions at electrode-electrolyte interface[48]. As can be observed, GNP/DB-GCE (curve ii) exhibited lower R_{ct} (31 Ω) than both of bare GCE (R_{ct}=243 Ω, curve i) and GNP-GCE (R_{ct}=112 Ω, curve iii) confirming the higher electrocatalytic activity of the GNP/DB nanocomposite film.

The stability of the GNP/DB-GCE was studied by repetitive CV measurements by potential sweeping between 0.0 and 0.7 V for 100 cycles at a scan rate of 50 mV/s. The CV background current of GNP/DB-GCE decreased slowly between 0.3 and 0.7 V, and after 100 cycles the electrode retained about 63% current (**Fig. S1**). This could be the result of the partial removal of GNP/DB from the electrode surface. We also tried to prepare GNP/DB film on a polyethylene terephthalate (PET) film using GNP/DB dispersion (*see experimental section 2.3*). After dry and multiple water washing steps, GNP/DB film remained strongly attached to the PET surface, which indicated that GNP/DB had relatively strong binding affinity to the hydrophobic surface (**Fig. S2**)[49].

3.3 Electrochemical oxidation of BPA

CVs of BPA in 125 mM PBS (pH 7) at bare and GNP- and GNP/DB-modified GCEs are shown in **Fig. 3a**. With bare GCE a small oxidation peak (at 0.551 V, 0.25 μA) was observed for BPA (curve i), whereas with GNP-GCE an unresolved oxidation peak was observed (curve ii). The oxidation peak current of BPA at GNP/DB-GCE is considerably improved (0.524 V, 1.71 μA) (curve iv). Without BPA, no such peak was observed at GNP/DB-GCE (curve iii); hence the

oxidation of BPA is undoubtedly attributed to the surface characteristics of the GNP/DB film structure. The response of GNP/DB-GCE was recorded at various BPA concentrations (**Fig. 3b**). The oxidation peak current increased linearly with increasing BPA concentration over the tested range of 2 to 36 μM (**Fig. 3c**).

Information about the electrochemical mechanism of BPA at the electrode interface can be acquired from the relationship between peak current and scan rate. **Fig. 4a** shows the CVs of 20 μM BPA at different scan rates of 0.01 to 0.15 V/s with GNP/DB-GCE. The oxidation peak was well resolved at low scan rates, but became increasingly broad and shifted towards more positive voltage with increasing scan rates, which suggests an irreversible electrode process. The relationship between the oxidation peak current (I_p, μA) and square root of scan rate (ν, V/s) was found to be linear (**Fig. 4c**):

$$I_p = 0.045\,\nu^{0.5} + +0.98 \qquad (R^2 = 0.9973)$$

This behavior suggests that the oxidation of BPA at GNP/DB is a diffusion-controlled process. A plot of anodic peak potential (E_{pa}) vs. natural logarithm of scan rate was also linear (**Fig. 4b**):

$$E_{pa} = 0.0297\,ln\nu + 0.476 \qquad (R^2 = 0.985)$$

For a totally irreversible electrode process, the relationship between E_{pa} and ln ν could be expressed as [50]:

$$E_{pa} = E^o + \frac{RT}{\propto nF} ln \frac{RTK^o}{\propto nF} + \frac{RT}{\propto nF} ln\,\nu$$

where α is the charge transfer coefficient, K^o is the standard rate constant of the reaction, *n* is the number of electron transfer involved in rate determining step, E^o is the formal redox potential, R is the ideal gas constant (8.314 J mol^{-1} K^{-1}), T is the absolute temperature (K), and F is the Faraday constant (96,485 C mol^{-1}). From the slope of E_{pa} vs. ln ν plot the value of αn was

calculated to be 0.926. However, in the irreversible oxidation process α was assumed 0.5 [51] indicating that *n*=2 for the oxidation of BPA at the GNP/DB-GCE.

The electrochemical behavior of BPA in aqueous medium is highly influenced by the pH of the solution. To optimize the pH, BPA concentration of 20 µM was tested in 125 mM PBS at pH 5.0 to 11.0 (**Fig. 4d**). The E_{pa} of BPA decreased with decreasing pH values (**Fig. 4d**). At pH 7, a high peak current with well resolved oxidation peak was obtained at a lower potential, thus pH 7 was chosen for optimization of BPA testing. The change in E_{pa} was linear against pH according to the following relationship (**Fig. 4d, inset**):

$$E_{pa} = 0.0618\, pH + 1.0415 \qquad (R^2 = 0.9965)$$

Thus, the slope of the pH regression equation (0.0618 V/pH) is close to the theoretical value of 0.0576 V/pH suggesting equal number of protons and electrons were involved in the electrode process[35]. This fact and the above discussion indicates that the electrochemical oxidation of BPA at GNP/DB-modified GCE is a two electrons and two protons process [50]. It is worth noting that a small cathodic peak appeared in low pH solutions in the potential range of -0.2 and 0.0 V which may be due to the functional groups of DB molecules attached with GNP (**Fig. 4d**). CVs of (i) bare GCE and (ii) GNP-GCE did not exhibit this cathodic peak at the same condition, so it should have come from the functional groups of DB.

Based on the above finding, a possible reaction mechanism of BPA at the GNP/DB-GCE can be suggested. The observed oxidation peak could be attributed to the anodic oxidation of the aromatic ring in BPA and the formation of resonance via a two-electron and two-proton process, and can be illustrated by **Scheme 2** [14]. The resulting products form during the oxidation are very unstable in the presence of nucleophiles and react immediately with aqueous solvent to form (I)

[36], which is a likely reason why electrochemically irreversible oxidation process was observed for BPA (Scheme 2).

3.4 Differential pulse voltammetry (DPV) study

DPV is a very sensitive and commonly used electroanalytical technique to determine trace level of elements[52]. **Fig. 5** shows the DPV oxidation peaks of BPA in 125 mM pH 7 PBS at various concentrations and the corresponding calibration curve. The peak current of BPA oxidation is linear over two BPA concentration ranges of: 10 nM to 100 nM

$$i_{pa} = 3.4\,C - 0.007 \qquad (R^2 = 0.9994)$$

and 100 nM to 25 µM.

$$i_{pa} = 0.40\,C + 0.25 \qquad (R^2 = 0.9976)$$

Where, C is the BPA concentration (µM) and i_{pa} is the oxidation peak current (µA). The current sensitivity of BPA is 0.4 µA/µM. The limit of detection (LOD) and limit of quantification (LOQ) were calculated as 3.3 SD/*b* and 10 SD/*b*, respectively, where SD is the standard deviation of five reagent blank determinations and *b* is the slope of the calibration curve[53]. For GNP/DB-GCE, the LOD and LOQ were 1.23 nM and 3.73 nM, respectively. This LOD is lower than what was obtained in some other electrochemical methods, e.g., molecularly imprinted chitosan–graphene composite modified electrode (~6 nM)[54] and almost similar to the results obtained using single-walled carbon nanotubes conjugated with β-cyclodextrin (1.0 nM) [55] or reduced graphene oxide/carbon nanotube/gold nanoparticles nanocomposite functionalized screen-printed electrode (0.8 nM)[36]. The performance comparison of our sensor and several that have been reported in the literature (**Table 2)** indicate that our sensor reports low LOD and wide linear range and could potentially be used for sensitive detection of BPA. Furthermore, our sensor also exhibited better stability and reproducibility with relative standard deviation (RSD)

of 0.46 % for five successive measurements of 10 μM BPA on the same electrode and in pH 7.0 PBS.

The specificity of our sensor was evaluated in the presence of other organic and inorganic species which are usually present along with BPA. The interference effect was calculated as:

$$Interference\ (\%) = \frac{I_{BPA} - I_{BPA\ +\ Interferent}}{I_{BPA}} \times 100$$

Where, I_{BPA} = oxidation peak current for BPA, $I_{BPA+interferent}$ = oxidation peak current for BPA plus added interferent. The results presented in **Table 3** demonstrate that BPA measurements (10 μM in pH 7 PBS) were unaffected (peak current change <5%) by the presence of about 100-fold concentrations of H_2O_2, ascorbic acid, citric acid, oxalic acid, glucose, caffeine, Mg^{2+}, Ca^{2+}, SO_4^{2-}; and 10-fold concentrations of Fe^{2+}, Cu^{2+}, Zn^{2+}, and Hg^{2+}.

3.5 Analysis of real samples

We also tested our sensor for its effectiveness in determining trace amount of BPA in different commercial milk and juice samples. These samples, at our detection limit, were all free of BPA; thus they were spiked with known amounts of BPA standard solution. The results (**Table 4**) indicate that our sensor is a promising device for practical testing for BPA in real matrices.

3.6 Electrochemical response of GNP/DB modified electrodes towards H_2O_2 reduction

Biologically, it has been established that H_2O_2 acts upon eukaryotic signal transduction, which is generated in response to various stimuli, and is involved in regulating diversity of biological processes in mammals and in plants [56]. These biological activities underscore the importance of H_2O_2 monitoring.

CV responses of bare and GNP- or GNP/DB-modified GCEs towards the reduction of 1 mM H_2O_2 are shown in **Fig. 6a**. The reduction signal at GNP/DB-GCE shows a much higher

peak at additional positive potential when compared to those of bare and GNP-modified GCE. The GNP-GCE produced a peak current (curve ii) at about -0.9 V, this peak was significant as compared to bare GCE (curve iii). The production of this peak could be due to the introduction of graphene nanomaterial that can increase the electroactive surface area of the electrode[52, 57]. In comparison GNP/DB-GCE showed a prominent increase in the current peak appeared at about -400 mV (curve i). The results are in agreement with those obtained when H_2O_2 characterized at nitrogen-doped graphene[32], thus explain that the improvement of the electrocatalytic activity mainly contributes to the presence of nitrogen groups in the DB molecules that doped on graphene.

Amperometry, a fast and sensitive electroanalytical technique[58], was used to evaluate the change in current response as a function of time. Typical amperometric response of GNP/DB-GCE recorded at successive additions of H_2O_2 at a static potential of -400 mV vs. Ag/AgCl is presented in **Fig. 6b**. When the background current was stable, different concentrations of H_2O_2 were injected into the electrolyte under stirring (~300 rpm). The sensor response increased rapidly to a steady level within 2 s. Such a fast response can be attributed to the high electro-catalytic activity of DB with graphene nanomaterials. The detection limit achieved was 5.6 μM. The calibration plot (**Fig. 6c)**, shows a highly linear (R^2=0.998) increase in signal with increase in H_2O_2 concentration in the range of 10 μM to 1.9 mM with a sensitivity of 57.6 $\mu A.mM^{-1}$.

4. Conclusions

GNP are dispersed in water with the assistance of DB, a tri-azo dye, and the GNP/DB dispersion was used to deposit GNP/DB nanocomposite film on GCE. This sensor (GNP/DB-GCE) exhibited high electrocatalytic activity to BPA and H_2O_2. DPV peak current of BPA oxidation is linear over two BPA concentration ranges of 10 nM to 100 nM and 100 nM to 25

μM. The LOD of BPA was 1.23 nM, and the sensor performance was unaffected by a number of interfering organic and inorganic compounds. BPA detection was also validated in real matrices using spiked milk and fruit juice samples. Electrocatalytic reduction of H_2O_2 at GNP/DB-GCE was performed and used to detect H_2O_2 in the range of 10 μM to 1.9 mM, with a LOD of 5.6 μM; it also exhibited a fast amperometric response of less than 2 s. Thus, our sensor has the potential for sensitive detection of both BPA and H_2O_2.

Acknowledgments

This work was supported in part by funding from the National Institute of Food and Agriculture, United States Department of Agriculture, under ID number WIS01644. The Authors acknowledge the use of instrumentation supported by the UW MRSEC (DMR-1121288) and the UW NSEC (DMR-0832760). Author NGY would like to thank the Scholar Rescue Fund Fellowship for their support.

References

1. H. Hiroi, O. Tsutsumi, M. Momoeda, Y. Takai, Y. Osuga and Y. Taketani, *Endocrine Journal*, 1999, **46**, 773-778.
2. L. N. Vandenberg, M. V. Maffini, C. Sonnenschein, B. S. Rubin and A. M. Soto, *Endocrine Reviews*, 2009, **30**, 75-95.
3. J. M. Braun and R. Hauser, *Current Opinion in Pediatrics*, 2011, **23**, 233-239.
4. O. Ros, A. Vallejo, L. Blanco-Zubiaguirre, M. Olivares, A. Delgado, N. Etxebarria and A. Prieto, *Talanta*, 2015, **134**, 247-255.
5. A. Dang, M. Sieng, J. J. Pesek and M. T. Matyska, *Journal of Liquid Chromatography & Related Technologies*, 2014, **38**, 438-442.
6. L. Du, C. Zhang, L. Wang, G. Liu, Y. Zhang and S. Wang, *Microchim Acta*, 2015, **182**, 539-545.
7. X. Tu, L. Yan, X. Luo, S. Luo and Q. Xie, *Electroanalysis*, 2009, **21**, 2491-2494.
8. H.-s. Yin, Y.-l. Zhou and S.-y. Ai, *Journal of Electroanalytical Chemistry*, 2009, **626**, 80-88.
9. V. Chauke, F. Matemadombo and T. Nyokong, *Journal of Hazardous Materials*, 2010, **178**, 180-186.
10. H. Yin, L. Cui, Q. Chen, W. Shi, S. Ai, L. Zhu and L. Lu, *Food Chemistry*, 2011, **125**, 1097-1103.
11. M. Najafi, M. A. Khalilzadeh and H. Karimi-Maleh, *Food Chemistry*, 2014, **158**, 125-131.
12. H. Yin, L. Cui, S. Ai, H. Fan and L. Zhu, *Electrochimica Acta*, 2010, **55**, 603-610.
13. Q. Li, H. Li, G.-F. Du and Z.-H. Xu, *Journal of Hazardous Materials*, 2010, **180**, 703-709.

14. L. Peng, S. Dong, H. Xie, G. Gu, Z. He, J. Lu and T. Huang, *Journal of Electroanalytical Chemistry*, 2014, **726**, 15-20.
15. S. Jiao, J. Jin and L. Wang, *Talanta*, 2014, **122**, 140-144.
16. S. A. Kumar, P.-H. Lo and S.-M. Chen, *Nanotechnology*, 2008, **19**, 255501.
17. P.-H. Lo, S. A. Kumar and S.-M. Chen, *Colloids and Surfaces B: Biointerfaces*, 2008, **66**, 266-273.
18. R. F. P. Nogueira, M. C. Oliveira and W. C. Paterlini, *Talanta*, 2005, **66**, 86-91.
19. N. G. Yasri, H. Seddik and M. A. Mosallb, *Arabian Journal of Chemistry*, 2015, **8**, 487-494.
20. J. Yuan and A. M. Shiller, *Analytical Chemistry*, 1999, **71**, 1975-1980.
21. K. Zhou, Y. Zhu, X. Yang, J. Luo, C. Li and S. Luan, *Electrochimica Acta*, 2010, **55**, 3055-3060.
22. S. Nandini, S. Nalini, R. Manjunatha, S. Shanmugam, J. S. Melo and G. S. Suresh, *Journal of Electroanalytical Chemistry*, 2013, **689**, 233-242.
23. A. K. Geim and K. S. Novoselov, *Nat Mater*, 2007, **6**, 183-191.
24. S. J. Amirfakhri, D. Binny, J.-L. Meunier and D. Berk, *Journal of Power Sources*, 2014, **257**, 356-363.
25. X. Huang, Y. Zhao, Z. Ao and G. Wang, *Scientific Reports*, 2014, **4**, 7557.
26. D. Pullini, V. Siong, D. Tamvakos, B. L. Ortega, M. F. Sgroi, A. Veca, C. Glanz, I. Kolaric and A. Pruna, *Composites Science and Technology*, 2015, **112**, 16-21.
27. D. Li, M. B. Muller, S. Gilje, R. B. Kaner and G. G. Wallace, *Nat Nano*, 2008, **3**, 101-105.
28. C. Li and G. Shi, *Advanced Materials*, 2014, **26**, 3992-4012.
29. A. K. Sundramoorthy and S. Gunasekaran, *Electroanalysis*, 2015, **27**, 1811-1816.
30. A. K. Sundramoorthy, Y. Wang, J. Wang, J. Che, Y. X. Thong, A. C. W. Lu and M. B. Chan-Park, *Scientific Reports*, 2015, **5**, 10716.
31. H. Lim, J. S. Lee, H.-J. Shin, H. S. Shin and H. C. Choi, *Langmuir*, 2010, **26**, 12278-12284.
32. Y. Wang, Y. Shao, D. W. Matson, J. Li and Y. Lin, *ACS nano*, 2010, **4**, 1790-1798.
33. J. Liang, Y. Jiao, M. Jaroniec and S. Z. Qiao, *Angewandte Chemie International Edition*, 2012, **51**, 11496-11500.
34. M. Seong and D. S. Kim, *Journal of Applied Polymer Science*, 2015, **132**, 42269.
35. X. Q. Liu, R. Yan, J. Zhu, J. M. Zhang and X. H. Liu, *Sensors and Actuators B-Chemical*, 2015, **209**, 328-335.
36. M. Li, Y. Yu, J. Li, B. Chen, A. Konarov and P. Chen, *Journal of Power Sources*, 2015, **293**, 976-982.
37. J. E. Park, G.-H. Lee, H.-W. Shim, D. W. Kim, Y. Kang and D.-W. Kim, *Electrochemistry Communications*, 2015, **57**, 39-42.
38. A. K. Sundramoorthy, S. Mesgari, J. Wang, R. Kumar, M. A. Sk, S. H. Yeap, Q. Zhang, S. K. Sze, K. H. Lim and M. B. Chan-Park, *Journal of the American Chemical Society*, 2013, **135**, 5569-5581.
39. S. Mesgari, A. K. Sundramoorthy, L. S. Loo and M. B. Chan-Park, *Faraday Discussions*, 2014, **173**, 351-363.
40. C. Peng, Y. Xiong, Z. Liu, F. Zhang, E. Ou, J. Qian, Y. Xiong and W. Xu, *Applied Surface Science*, 2013, **280**, 914-919.
41. P. Huang, L. Jing, H. Zhu and X. Gao, *Accounts of Chemical Research*, 2012, **46**, 43-52.
42. D. C. Elias, R. R. Nair, T. M. Mohiuddin, S. V. Morozov, P. Blake, M. P. Halsall, A. C. Ferrari, D. W. Boukhvalov, M. I. Katsnelson, A. K. Geim and K. S. Novoselov, *Science*, 2009, **323**, 610-613.
43. Z. Ni, Y. Wang, T. Yu and Z. Shen, *Nano Res.*, 2008, **1**, 273-291.
44. M. A. Pimenta, G. Dresselhaus, M. S. Dresselhaus, L. G. Cancado, A. Jorio and R. Saito, *Physical Chemistry Chemical Physics*, 2007, **9**, 1276-1290.
45. G. L. C. Paulus, Q. H. Wang and M. S. Strano, *Accounts of Chemical Research*, 2012, **46**, 160-170.
46. A. C. Ferrari, *Solid State Communications*, 2007, **143**, 47-57.
47. C. T. J. Low, F. C. Walsh, M. H. Chakrabarti, M. A. Hashim and M. A. Hussain, *Carbon*, 2013, **54**, 1-21.

48. J. Yang and S. Gunasekaran, *Carbon*, 2013, **51**, 36-44.
49. A. Sundramoorthy, Y.-C. Wang and S. Gunasekaran, *Nano Res.*, 2015, DOI: 10.1007/s12274-015-0880-1, 1-16.
50. W. Zhou, C. Sun, Y. Zhou, X. Yang and W. Yang, *Food Chemistry*, 2014, **158**, 81-87.
51. X. Wang, L. Yang, X. Jin and L. Zhang, *Food Chemistry*, 2014, **157**, 464-469.
52. N. Yasri, A. K. Sundramoorthy, W.-J. Chang and S. Gunasekaran, *Frontiers in Materials*, 2014, **1**, 33.
53. A. Shrivastava and V. Gupta, *Chronicles of Young Scientists*, 2011, **2**, 21-25.
54. P. Deng, Z. Xu and Y. Kuang, *Food Chemistry*, 2014, **157**, 490-497.
55. Y. Gao, Y. Cao, D. Yang, X. Luo, Y. Tang and H. Li, *Journal of Hazardous Materials*, 2012, **199–200**, 111-118.
56. E. A. Veal, A. M. Day and B. A. Morgan, *Molecular Cell*, 2007, **26**, 1-14.
57. A. K. Sundramoorthy and S. Gunasekaran, *TrAC, Trends Anal. Chem.*, 2014, **60**, 36-53.
58. N. G. Yasri, A. J. Halabi, G. Istamboulie and T. Noguer, *Talanta*, 2011, **85**, 2528-2533.
59. C. Yu, L. Gou, X. Zhou, N. Bao and H. Gu, *Electrochimica Acta*, 2011, **56**, 9056-9063.
60. G. F. Pereira, L. S. Andrade, R. C. Rocha-Filho, N. Bocchi and S. R. Biaggio, *Electrochimica Acta*, 2012, **82**, 3-8.
61. X. Yu, Y. Chen, L. Chang, L. Zhou, F. Tang and X. Wu, *Sensors and Actuators B: Chemical*, 2013, **186**, 648-656.

Tables

Table 1. Raman vibrational bands of different GNP samples and their intensity ratios.

Sample	Wavenumber (cm^{-1})			I_D/I_G	I_{2D}/I_G	Reference
	D	G	2D			
GNP	1364	1585	2734	0.159	0.373	This work
GNP/DB film	1380	1593	2751	0.62	0.231	This work
Annealed GNP/DB film	1374	1603	2757	0.18	0.376	This work
Graphite (pencil)	1311	1583	2629	0.067	--	[29]
Graphene (single-layer)	1333	1587	2658	0.11	1.7	[16, 17]
3,5-TBD/Gn *	1315	1580	2629	2.4	0.2	[17]
Dz/Gn **	--	1,591.9	2,649.8	1.42	1.64	[29, 45]
GO †	1352	1594	2935	0.75	--	[29]

* 3,5-TBD/Gr is 1 mM 3,5-bis-tert-butylbenzenediazonium grafted to single layer graphene,
** Dz/Gn is diazonium functionalized single-layer graphene.
† GO is graphene oxide

Table 2. Performance of different electrochemical BPA sensors reported in the literature

Method	**Electrode***	**Linear range**	**Limit of detection (nM)**	**Reference**
Amperometry	SWCNT-CD/GCE	10.8 nM –18.5 μM	1	Gao *et al.* [55]
DPV	ChS-Fe_3O_4/GCE	50 nM–30 μM	8	Yu *et al.*[59]
DPV	BDD electrode	440 nM–5.2 μM	2100	Pereira *et al.*[60]
DPV	Mg-Al-CO_3 LDH/GCE	10 nM−1.05 μM	5	Yin *et al.*[12]
DPV	CD-ILB/CPE	100 nM −11 μM	83	Yu *et al.*[61]
Derivative voltammetry	MIP ChS-Gr/ABPE	8 nM−1 μM;1 −20 μM	6	Deng *et al.*[54]
DPV	GNP/DB-GCE	10 nM–25 μM	1.23	Present work

*ChS, chitosan; Fe_3O_4, iron oxide; GCE, glassy carbon electrode; BDD, boron-doped diamond; SWCNT, single-walled carbon nanotubes; CD, β-cyclodextrin; Mg, magnesium; Al, aluminium; CO_3, carbonate; LDH, layered double hydroxide; ILB/CPE, ionic liquid-based carbon paste electrode; MIP ChS, molecularly imprinted chitosan; Gr, graphene; ABPE, acetylene black paste electrode.

Table 3. Interference of different organic and inorganic species on the DPV measurement of 10 μM BPA in pH 7 PBS using GNP/DB-GCE (n=5).

Material	**Ratio of interfering Material/BPA**	**BPA measured (μM) (mean± SD)**	**RSD (%)**	**Interference (%)**
BPA	--	10.02 ± 0.112	1.83	0.0
H_2O_2	100	9.79 ± 0.21	2.07	-2.15
Ascorbic acid	100	9.88 ± 0.20	2.03	-1.17
Oxalic acid	100	9.73 ± 0.36	3.71	-2.66
Glucose	100	9.76 ± 0.14	1.43	-2.40
Caffeine	100	9.90 ± 0.11	1.14	-0.90
Mg^{2+}	100	10.13 ± 0.26	2.56	1.25
Ca^{2+}	100	9.79 ± 0.31	3.21	-2.06
SO_4^{2-}	100	9.53± 0.14	1.45	-4.71
Fe^{2+}	10	9.82± 0.45	4.54	-1.76
Cu^{2+}	10	9.77± 0.22	2.22	-2.30
Zn^{2+}	10	9.68± 0.43	4.45	-3.21
Hg^{3+}	10	10.44± 0.36	3.41	+4.36

Table 4. DPV determination of BPA in spiked milk and juice samples (n = 5).

Sample*	**BPA added ($\times 10^{-7}$ M)**	**BPA measured mean ± SD ($\times 10^{-7}$ M)**	**Recovery (%)**	**RSD (%)**
Pasteurized milk	5.0	5.11 ± 0.08	102.2	2.62
Pasteurized milk with vitamin D	10.0	9.92 ± 0.12	99.2	2.29
Cranberry juice	10.0	10.32 ± 0.09	103.2	1.65
Lemonade	20.0	20.41 ± 0.14	102.1	1.93

*Store-bought samples did not contain any BPA as measured with our sensor.

Schemes and Figures

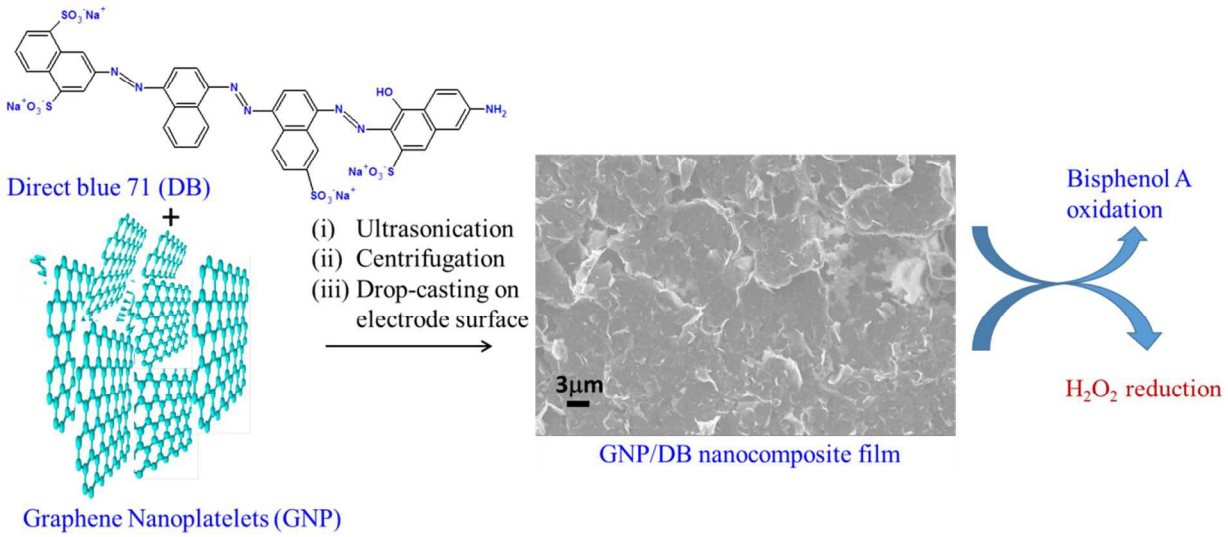

Scheme 1. GNP are dispersed in water with the aid of DB and the GNP/DB nanocomposite film was used for electrochemical oxidation of BPA and reduction of H_2O_2.

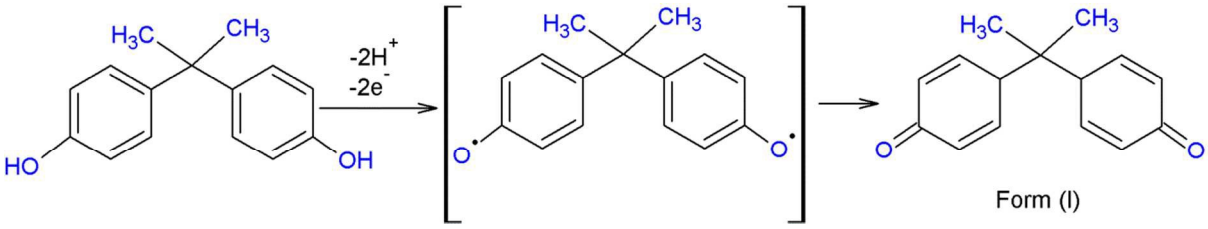

Scheme 2. The electrochemical oxidation mechanism of BPA at GNP/DB-modified electrode.

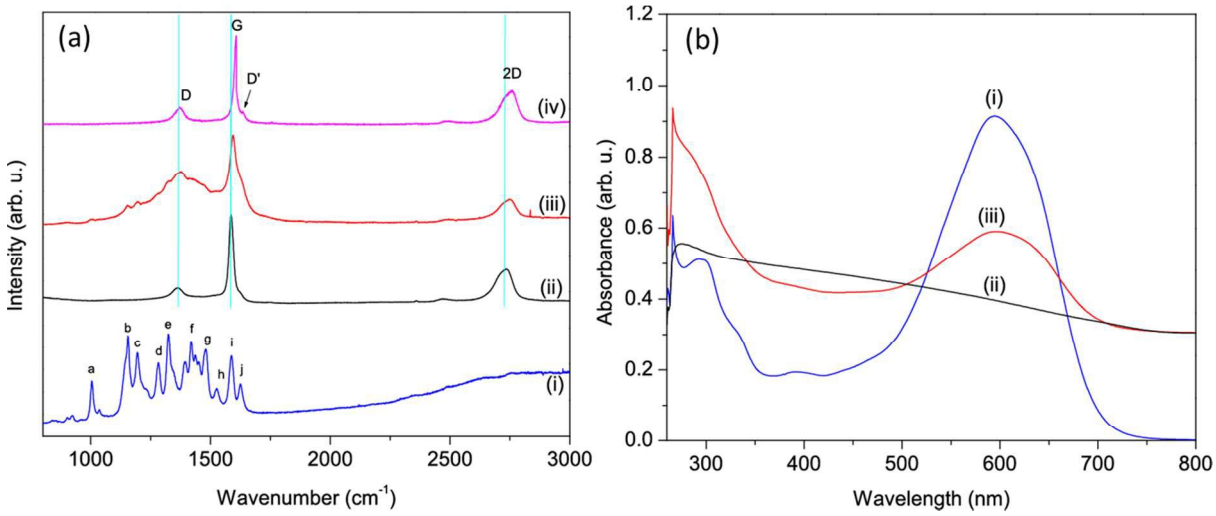

Figure 1. (a) Raman spectra of (i) DB, (ii) GNP, (iii) GNP/DB and (iv) GNP/DB film after thermal annealing. **(b)** UV-vis spectra of (i) DB, (ii) GNP and (iii) GNP/DB dispersions in DMF.

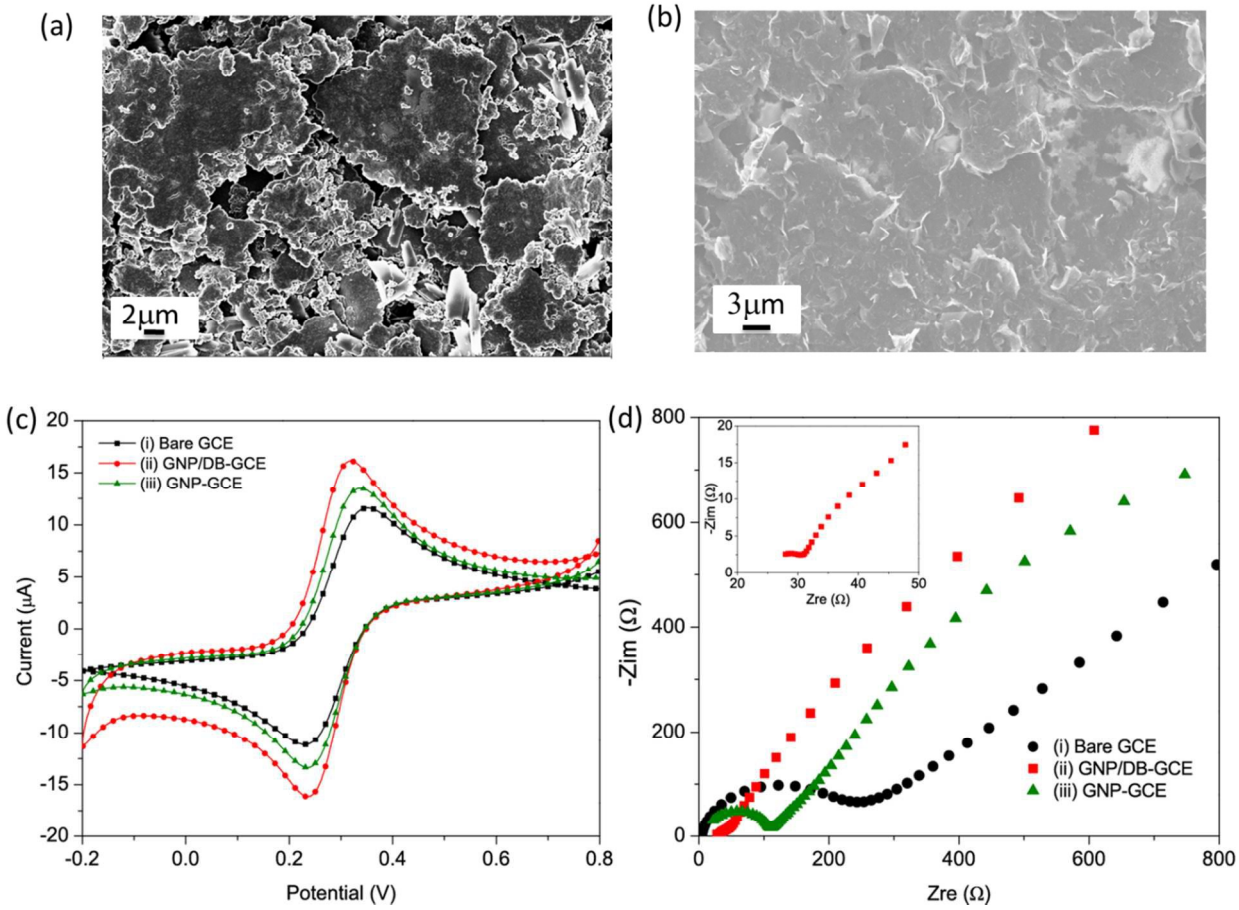

Figure 2. SEM images of **(a)** pristine GNP and **(b)** GNP/DB film. Cyclic Voltammogram **(c)** and Nyquist plots **(d)** of (i) bare GCE, (ii) GNP/DB-GCE, and (iii) GNP-GCE (Inset is enlarged Nyquist plot of (ii) GNP/DB-GCE). Supporting electrolyte: 2.5 mM $[Fe(CN)_6]^{4-/3-}$ + 0.1 M KCl. Scan rate: 20 mV/s.

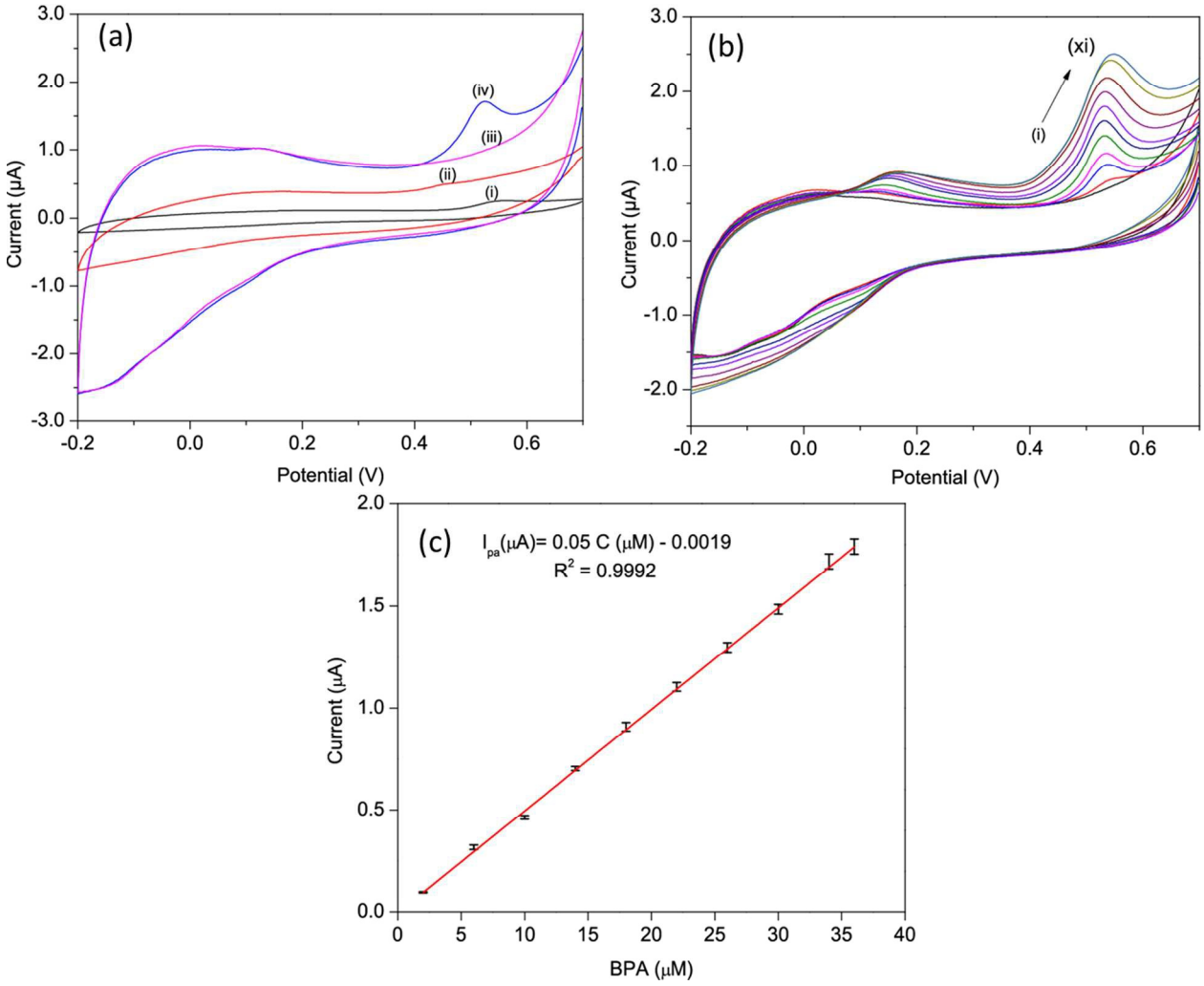

Figure 3. (a) Cyclic voltammograms of 10 μM BPA at (i) bare GCE, (ii) GNP-GCE and (iv) GNP/DB-GCE and (iii) GNP/DB-GCE in the absence of BPA **(b)** Cyclic voltammograms of GNP/DB-GCE for BPA concentrations (C, μM) of: (i) 0, (ii) 2, (iii) 6, (iv) 10, (v) 14, (vi) 18, (vii) 22, (viii) 26 (ix) 30, (x), 34, and (xi) 36**. (c)** Calibration plot of BPA (data points are means of four measurements each). Supporting electrolyte was 125 mM PBS, pH 7. Scan rate = 20 mV/s.

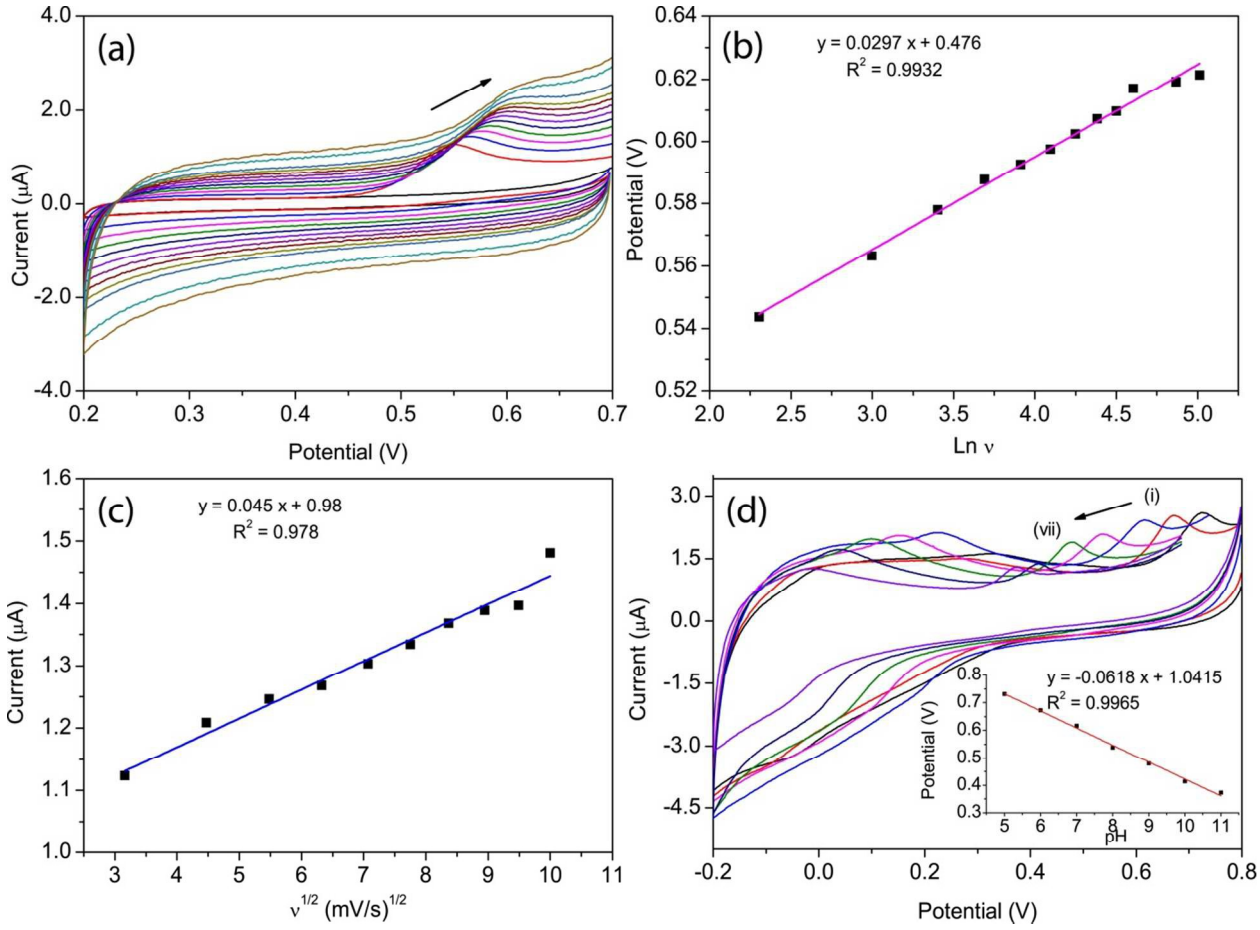

Figure 4. **(a)** Cyclic voltammograms of 20 μM BPA were recorded using GNP/DB-GCE at scan rates from 0.01 to 0.150 V/s (inner to outer), **(b)** Natural logarithm of scan rate (ν) vs potential, and **(c)** square root of scan rate ($\nu^{1/2}$) vs oxidation peak currents, **(d)** Cyclic voltammograms of 20 μM BPA at different pH (from pH = 11 (i) to pH =5 (vii)) (Inset: oxidation potential vs. pH). Supporting electrolyte= pH 7.0 PBS.

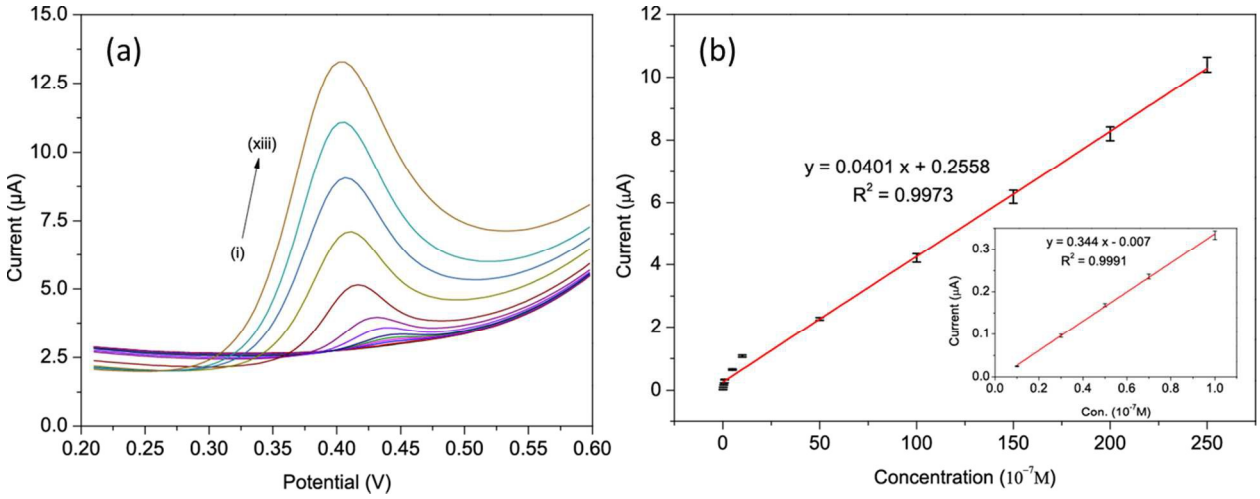

Figure 5. (a) DPV curves of GNP/DB-GCE in pH 7.0 PBS for different BPA concentrations ($\times 10^{-7}$ M): (i) 0.1, (ii) 0.3, (iii) 0.5, (iv) 0.7, (v) 1.0, (vi) 5.0, (vii) 10.0, (viii) 50.0, (ix) 75.0, (x) 100.0, (xi) 150.0, (xii) 200.0, and (xiii) 250. Step Potential = 0.005 V, amplitude = 0.05 V, interval time = 0.5 s, scan rate = 0.01 V/s; **(b)** peak current vs. BPA concentration calibration curve (data points are means of four measurements each). (inset: BPA concentration range of 0.1 - 1.0×10^{-7} M).

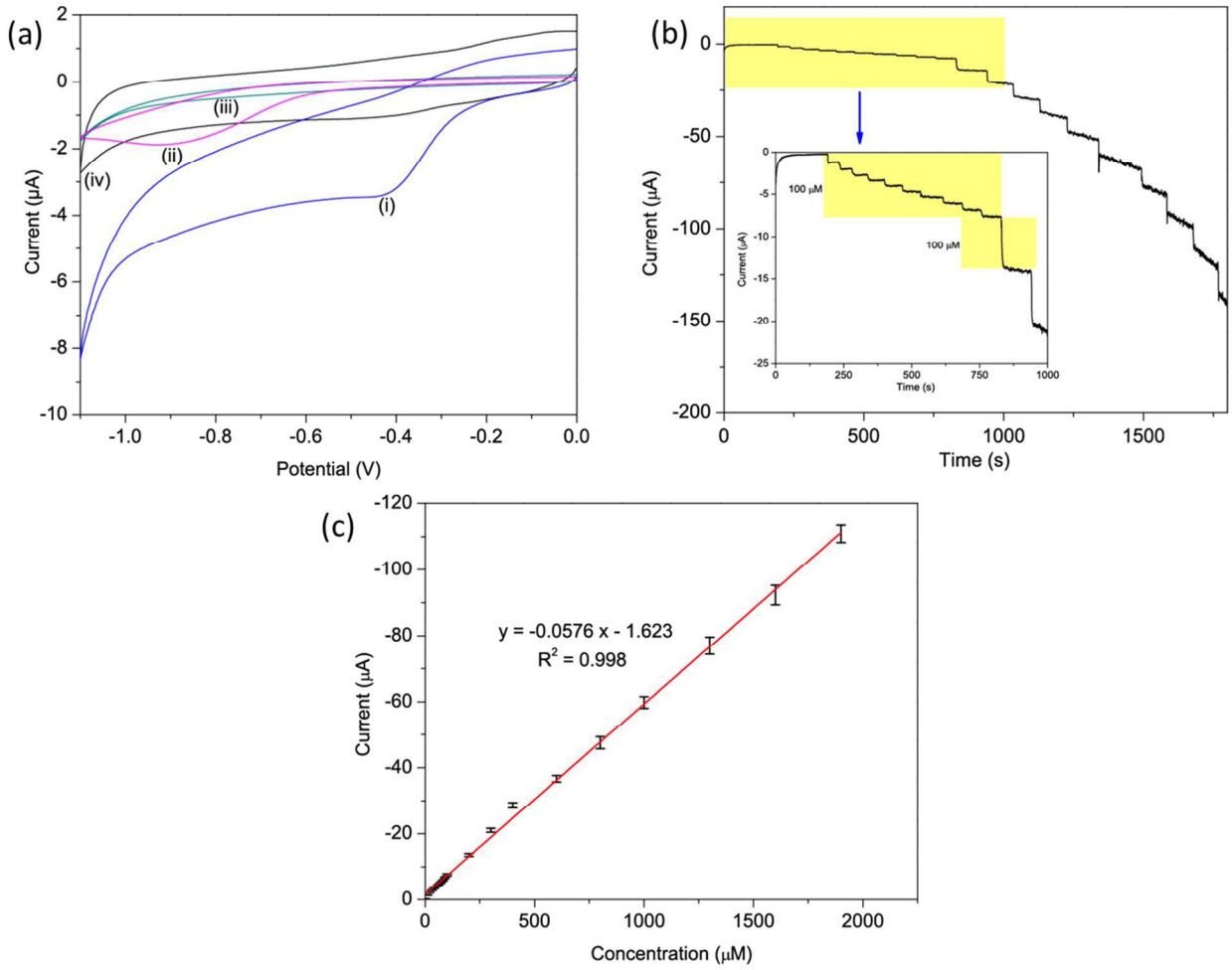

Figure 6. (a) Cyclic voltammograms in 125 mM pH 7 PBS for (i) GNP/DB-GCE, (ii) GNP-GCE, and (iii) bare GCE with 1 mM H_2O_2 and for (iv) GNP/DB-GCE without H_2O_2. Scan rate 20 mV/s. **(b)** Chronoamperometric response of GNP/DB-GCE to successive additions of H_2O_2 in 125 mM pH 7 PBS. Inset: magnified view at low concentration range. Applied potential= -400 mV. **(c)** Current vs. H_2O_2 concentration calibration curve (data points are means of four measurements each). All experiments were performed in N_2-saturated solution.

TOC graphic:

A new electrochemical sensor is developed based on graphene nanoplatelets functionalized with tri-azo dye (Direct blue 71) for selective and highly sensitive detection of bisphenol A and hydrogen peroxide in pH 7 phosphate buffered saline solution.